LLNL-JRNL-642086

LAWRENCE
LIVERMORE
NATIONAL
LABORATORY

NUSTAR OBSERVATIONS OF MAGNETAR 1E 1841-045

H. An, R. Hascoet, V. M. Kaspi, A. M. Beloborodov, F. Dufour, E. V. Gotthelf, R. Archibald, M. Bachetti, S. E Boggs, F. E. Christensen, W. W. Craig, B. W Greffenstette, C. J. Hailey, F. A. Harrison, T. Kitaguchi, C. Kouveliotou, K. K. Madsen, C. B. Markwardt, D. Stern, J. K. Vogel, W. W. Zhang

August 8, 2013

The Astrophysical Journal

Disclaimer

This document was prepared as an account of work sponsored by an agency of the United States government. Neither the United States government nor Lawrence Livermore National Security, LLC, nor any of their employees makes any warranty, expressed or implied, or assumes any legal liability or responsibility for the accuracy, completeness, or usefulness of any information, apparatus, product, or process disclosed, or represents that its use would not infringe privately owned rights. Reference herein to any specific commercial product, process, or service by trade name, trademark, manufacturer, or otherwise does not necessarily constitute or imply its endorsement, recommendation, or favoring by the United States government or Lawrence Livermore National Security, LLC. The views and opinions of authors expressed herein do not necessarily state or reflect those of the United States government or Lawrence Livermore National Security, LLC, and shall not be used for advertising or product endorsement purposes.

Draft version August 5, 2013
Preprint typeset using LaTeX style emulateapj v. 12/16/11

NUSTAR OBSERVATIONS OF MAGNETAR 1E 1841−045

Hongjun An[1], Romain Hascoët[2], Victoria M. Kaspi[1,13], Andrei M. Beloborodov[2], François Dufour[1], Eric V. Gotthelf[2], Robert Archibald[1], Matteo Bachetti[3,4], Steven E. Boggs[5], Finn E. Christensen[6], William W. Craig[5,7], Brian W. Greffenstette[8], Charles J. Hailey[2], Fiona A. Harrison[8], Takao Kitaguchi[9], Chryssa Kouveliotou[10], Kristin K. Madsen[8], Craig B. Markwardt[11], Daniel Stern[12], Julia K. Vogel[7], and William W. Zhang[11]

[1]Department of Physics, McGill University, Montreal, Quebec, H3A 2T8, Canada
[2]Columbia Astrophysics Laboratory, Columbia University, New York NY 10027, USA
[3]Université de Toulouse, UPS-OMP, IRAP, Toulouse, France
[4]CNRS, Institut de Recherche en Astrophysique et Planétologie, 9 Av. colonel Roche, BP 44346, F-31028 Toulouse Cedex 4, France
[5]Space Sciences Laboratory, University of California, Berkeley, CA 94720, USA
[6]DTU Space, National Space Institute, Technical University of Denmark, Elektrovej 327, DK-2800 Lyngby, Denmark
[7]Lawrence Livermore National Laboratory, Livermore, CA 94550, USA
[8]Cahill Center for Astronomy and Astrophysics, California Institute of Technology, Pasadena, CA 91125, USA
[9]RIKEN, 2-1 Hirosawa, Wako, Saitama, 351-0198, Japan
[10]Space Science Office, ZP12, NASA Marshall Space Flight Center, Huntsville, AL 35812, USA
[11]Goddard Space Flight Center, Greenbelt, MD 20771, USA
[12]Jet Propulsion Laboratory, California Institute of Technology, Pasadena, CA 91109, USA

Draft version August 5, 2013

ABSTRACT

We report new spectral and temporal observations of the magnetar 1E 1841−045 in the Kes 73 supernova remnant obtained with the *Nuclear Spectroscopic Telescope Array* (NuSTAR). Combined with new *Swift* and archival *XMM-Newton* and *Chandra* observations, the phase-averaged spectrum is well characterized by a blackbody plus double power-law model, in agreement with previous, multi-mission X-ray results. However, we are unable to reproduce the unique spectral results reported using *Suzaku* observations. The pulsed fraction of the source is found to increase with photon energy, implying that the pulsed spectrum above 15 keV is significantly harder than the total (pulsed and unpulsed) spectrum. The measured rms pulsed fraction is ∼12% and ∼17% at ∼20 keV and ∼50 keV, respectively. We detect a new feature in the 24–35 keV band pulse profile that is uniquely double-peak. This feature may be associated with a possible absorption or emission feature in the phase-resolved spectrum. We fit the X-ray data using the recently developed electron-positron outflow model of Beloborodov (2013) for the hard X-ray emission from magnetars. This produced a satisfactory fit allowing a constraint on the angle between the rotation and magnetic axes of the neutron star of ∼20° and on the angle between the rotation axis and line-of-sight of ∼50°. In this model, the soft X-ray component is inconsistent with a single blackbody; adding a second blackbody or a power-law component fits the data. The two-blackbody interpretation suggests a hot spot of temperature $kT \approx 0.9$ keV occupying ∼1% of the stellar surface.

Keywords: pulsars: individual (1E 1841−045) – stars: magnetars – stars: neutron – X-rays: bursts

1. INTRODUCTION

Magnetars are isolated neutron stars whose X-ray luminosities are thought to be powered by the decay of their intense magnetic fields (Duncan & Thompson 1992; Thompson & Duncan 1996). They are observed as pulsating X-ray sources occasionally producing bright bursts on timescales as short as 10 ms, as well as major enhancements in the persistent emission lasting days to months (see Woods & Thompson 2006; Mereghetti 2008; Rea & Esposito 2011, for reviews). Magnetic fields inferred from magnetar spin-down rates in many cases exceed 10^{14} G (e.g., 1E 1841−045, SGR 1806−20; Vasisht & Gotthelf 1997; Kouveliotou et al. 1998), although weaker fields are suggested by recent observations of several magnetars (e.g., SGR 0418+5729, Swift J1822.3−1606; Rea et al. 2010; Livingstone et al. 2011; Rea et al. 2012; Scholz et al. 2012). There are 26 magnetars discovered until now including candidates (see Olausen & Kaspi, in preparation).[2]

The X-ray spectra of magnetars often require two or more components. The soft X-ray component (peak at ∼1 keV) is thought to be dominated by the surface emission from the neutron star and is likely modified by resonant scattering in the magnetosphere (Thompson et al. 2002). It may be fitted by an absorbed blackbody plus power law or sometimes by a two-blackbody model. The hard X-ray component (which peaks above 100 keV, Kuiper et al. 2006; Enoto et al. 2010) is believed to be generated in the magnetosphere. Its origin has been

[13] Lorne Trottier Chair; Canada Research Chair

[2] See the online magnetar catalog for a compilation of known magnetar properties, http://www.physics.mcgill.ca/∼pulsar/magnetar/main.html

Table 1
Summary of observations used in this work

Observatory	Obs. ID	Obs. Date (MJD)	Exposure (ks)	Mode[a]
Chandra[b]	730	51754	10.5	CC
XMM-Newton	0013340101	52552	3.9	FW/LW
XMM-Newton	0013340102	52554	4.4	FW/LW
Chandra[c]	6732	53946	24.9	TE
Swift	00080220003	56240	17.9	PC
NuSTAR	30001025002	56240	48.6	···

[a]PC: Photon Counting, TE: Timed Exposure, FW: Full Window, LW: Large Window, CC: Continuous Clocking.
[b]Used only for 1E 1841−045.
[c]Used only for Kes 73 because of pile-up.

discussed by several authors (Thompson & Beloborodov 2005; Heyl & Hernquist 2005; Baring & Harding 2007; Beloborodov & Thompson 2007). Recently, Beloborodov (2013) proposed a detailed model of hard X-ray emission from the relativistic outflow created by $e^{\pm}$ discharge near the neutron star.

The Galactic magnetar 1E 1841−045 is a located at the center of the shell-type X-ray and radio supernova remnant Kes 73, and was first identified as an anomalous X-ray pulsar by Vasisht & Gotthelf (1997). Its slow 11.8 s spin period and rapid spin-down rate implies a extreme magnetic field of $B \equiv 3.2\times10^{19}(P\dot{P})^{1/2}$ G $= 6.9\times10^{14}$ G, assuming the dipole spin-down model. Hard X-ray emission from 1E 1841−045/Kes 73 was detected by Molkov et al. (2004), and found to be highly pulsed (Kuiper et al. 2004, 2006), approaching 100% from 15–200 keV. Spectral studies by these authors showed that the hard power-law photon index ($\Gamma_{\rm h}$) is 1.32(11) in the ∼20–300 keV band measured with *RXTE* and *INTEGRAL*. However, Morii et al. (2010) described the spectrum with an absorbed blackbody plus two power-law model with typical values of $N_{\rm H} \approx 2.87\times10^{22}$ cm^{-2}, $kT \approx 0.54$keV, $\Gamma_{\rm s} \approx 5.0$ and $\Gamma_{\rm h} \approx 1.62$ using *Suzaku* data. The measurements reported using different observatories are marginally consistent over their various energy bands.

In this paper, we report on the spectral and temporal properties of 1E 1841−045 in the 0.5–79 keV band, measured with *NuSTAR*, the *Swift* X-ray telescope (XRT), *XMM-Newton*, and *Chandra*. In Section 2, we describe the observations used in this paper and in Section 3, we present the results of our data analysis. In Section 3.4, we use the our measurements of the hard X-ray emission from 1E 1841−045 to test the model of Beloborodov (2013) for the relativistic outflow created by $e^{\pm}$ discharge near the neutron star. We show that we are able to reproduce the specific predictions for the phase-resolved spectrum of the magnetar. Section 4 presents our discussion and conclusions. These are summarized in Section 5. Though this work, we assume the distance to 1E 1841−045/ Kes 73 to be 7.5–9.8 kpc, based on H I absorption measurements of Tian & Leahy (2008).

2. OBSERVATIONS

NuSTAR is the first satellite mission that has focusing capability above ∼10 keV (Harrison et al. 2013). It is composed of two focusing optics (Hailey et al. 2010) and two CdZnTe solid-state detectors (Harrison et al. 2010), where we use the terms "module A" and "module B" when referring to individual optics/detector sets. The observatory operates in the 3–79 keV band with energy resolution of 400 eV at 10 keV, angular resolution of 58″ (HPD, 18″ FWHM), and temporal resolution of 2 μs (see Harrison et al. 2013, for more details).

We began observing 1E 1841−045 with *NuSTAR* on 2012 November 9 for 48.6 ks at UT 22:00:02.184. Although *NuSTAR* is extremely sensitive in the hard X-ray band, a simultaneous 18-ks *Swift* XRT observation (PC mode) was conducted at UT 21:49:38.742 on 2012 November 9 to extend the data coverage down to ∼0.5 keV where the thermal component is dominant. A bright point source and extended emission out to ∼2′ in radius were clearly detected at the position consistent with that of 1E 1841−045/Kes 73.

The *NuSTAR* data were processed with `nupipeline` 1.1.1 along with CALDB version 20130509, and the *Swift* data with `xrtpipeline` along with the HEASARC remote CALDB[3] using the standard filtering procedure (Capalbi et al. 2005) to produce cleaned event files. We then further processed the cleaned event files for analysis as described below. We also analyzed archival *Chandra* and *XMM-Newton* observations to have better spectral sensitivity at low energies ($\lesssim$ 3 keV). The *Chandra* data were re-processed using `chandra_repro` of CIAO 4.4 along with CALDB 4.5.3, and the *XMM-Newton* data were processed with Science Analysis System (SAS) 12.0.1 (see Table 1 for a summary of all the observations on which we report).

3. DATA ANALYSIS AND RESULTS

3.1. *Timing Analysis*

We extracted source events in the 3–79 keV and 0.5–10 keV band within circular regions with radii 60″ and 20″ for *NuSTAR* and *Swift*, respectively, and applied a barycentric correction to the event lists using the `barycorr` tool with the orbit files and the clock correction files using the position reported by Wachter et al. (2004). We then used the H-test (de Jager et al. 1989) to search for pulsations and to measure the period. Pulsations were detected with very high significance, and the best periods (P) were 11.79130(2) s and 11.7914(2) s for the *NuSTAR* and the *Swift*, respectively. The uncertainties were estimated using the method given by Ransom et al. (2002). The periods we measured are consistent with those predicted on the basis of the ephemeris obtained with the *Swift* monitoring program that will be described elsewhere (Archibald, R. et al. in preparation).

Since we are measuring properties of 1E 1841−045, the Kes 73 background must be subtracted; to do this optimally, the background region should be within the remnant which is extended out to 120″ in radius from the neutron star. Extracting backgrounds from a magnetar-free region within Kes 73 was straightforward in the *Swift* data thanks to the XRT's good angular resolution; the backgrounds were extracted from an annular region with inner radius 60″ and outer radius 85″. However, extracting backgrounds was not easy in the *NuSTAR* data since the PSF is broad, and finding a source-free region within the remnant was not possible. Therefore, we extracted the background with inner and outer radii 60″ and 100″,

[3] http://heasarc.nasa.gov/docs/heasarc/caldb/caldb_remote_access.html

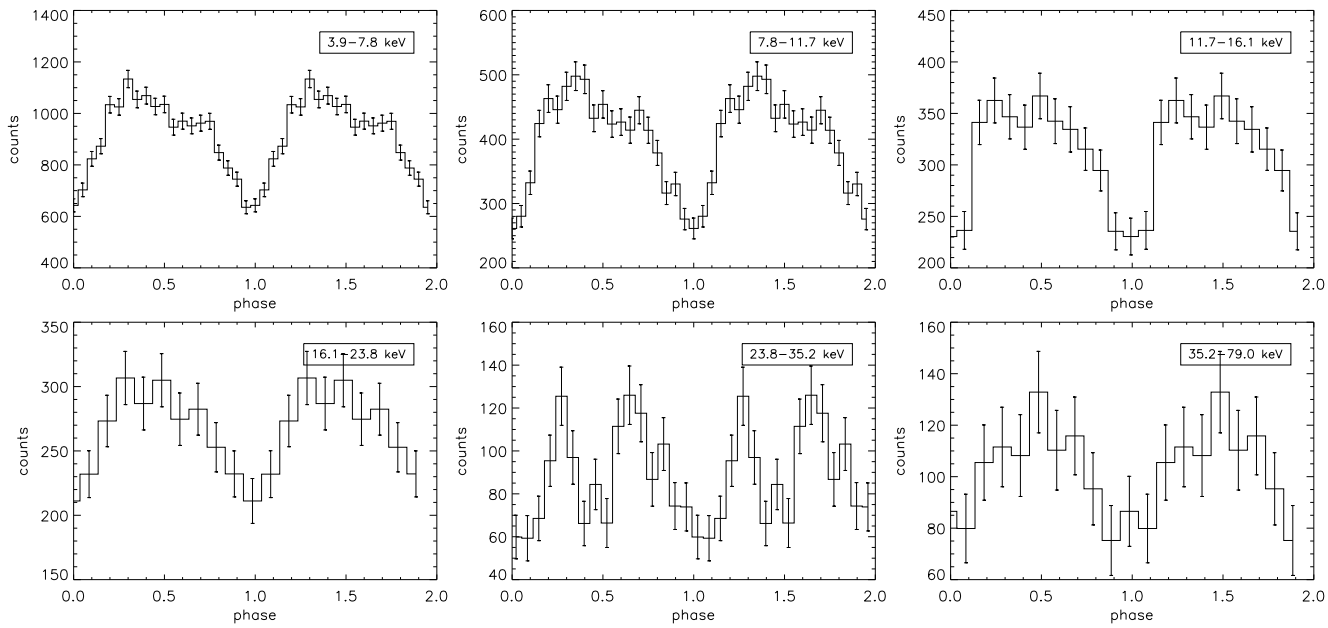

Figure 1. Pulse profiles for 1E 1841−045 from *NuSTAR* data in various energy bands. Note the different y-axis labels, as well as the suppressed zeros on the plots.

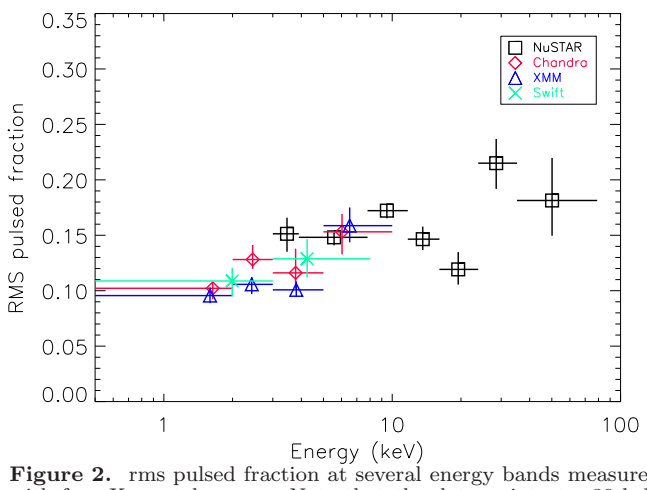

Figure 2. rms pulsed fraction at several energy bands measured with four X-ray telescopes. Note that the data point at ∼30 keV corresponds to the double-peaked structure in the pulse profile.

respectively, and then corrected for the source contamination in the background region (see Wang & Gotthelf 1998). The correction factor was calculated with *NuSTAR*'s instrument PSF and estimated to be ∼10% (Harrison et al. 2013).

We also analyzed archival *Chandra* and *XMM-Newton* observations. For the *Chandra* and *XMM-Newton* data, source events were extracted from a circle with radius 16″ and a rectangle with ∼3″ × 10″ (CC mode, 3″ along the event distribution), respectively. *XMM-Newton* backgrounds were extracted from events within an annular region with inner radius 48″ and outer radius 80″ centered at the source region, and *Chandra* backgrounds were extracted from two rectangular regions with ∼5″ × 10″ offset 5″ to each side from the source. We then applied barycentric corrections to all the event lists for temporal analysis below.

We folded the source event time series at the best measured period to produce pulse profiles for multiple energy bands. The background pulse profiles were produced in the same way using the background events and subtracted from the pulse profiles of the source regions to produce the source pulse profiles. The background-subtracted pulse profiles obtained with *NuSTAR* are plotted in Figure 1. The energy bands were chosen to enable comparison with those reported by Kuiper et al. (2004). For each energy band, the significance of pulsation was greater than 99%.

The pulse profiles in Fig. 1 qualitatively agree well with those reported by Kuiper et al. (2004). However, we see a double-peaked pulse profile in the 24–35 keV band measured with *NuSTAR*. The profile in this band has not been previously reported. To see if the apparent double peak occurred by chance due to binning effects, we tried 250 different binnings by varying the zero phase. For each trial binning, we fit the profile to two Gaussian functions, and measured the significance of each peak. In all 250 cases, the significance was greater than 3σ for both peaks. Moreover, the two peaks do not disappear when the energy range was adjusted slightly (e.g., 25–40 keV). Therefore, we conclude that the two peaks are genuine features in the light curve at this energy band.

We then calculated the pulsed fractions, defined as the ratio of total counts above the pulse minimum to the total counts for each energy band using the background-subtracted pulse profiles. The derived pulse fractions were highly dependent on the binning and the definition of pulse minimum. Therefore, we used an alternative definition (rms pulsed fraction),

$$PF_{\rm rms} = \frac{\sqrt{2\sum_{k=1}^{4}((a_k^2+b_k^2)-(\sigma_{a_k}^2+\sigma_{b_k}^2))}}{a_0},$$

where $a_k = \frac{1}{N}\sum_{i=1}^{N} p_i \cos(2\pi ki/N)$, σ_{a_k} is the uncertainty in a_k, $b_k = \frac{1}{N}\sum_{i=1}^{N} p_i \sin(2\pi ki/N)$, σ_{b_k} is the uncertainty in b_k, p_i is the number of counts in ith bin, N is the total number of bins, and n is the number of Fourier

harmonics included, in this case, $n = 4$ (see Gonzalez et al. 2010, for more details). We also performed similar analyses for the *XMM-Newton* and *Chandra* data and show the measured rms pulsed fractions in Figure 2. We find that the rms pulsed fraction increases fairly slowly with energy, reaching ∼20% around 50 keV.

We also searched for aperiodic variability with the *NuSTAR* data in the energy band from 3–79 keV. In particular, we searched for bursting activity in any energy band during the observations. We produced light curves with various time resolutions (0.1–1000 s) for several energy bands (e.g., 3–79 keV, 15–79 keV, 24–35 keV). We then searched for time bins having a significantly larger than average number of events accounting for the number of trials, but found none. Therefore, we conclude that there was no bursting activity on time scales of 0.1–1000 s during the observations.

3.2. *Phase-Averaged Spectral Analysis*

We extracted the source and the background events using the same regions defined in Section 3.1. To see if the *Swift* observation was piled-up, we measured the count rate within a circle of radius 20 pixels (∼47″).[4] The count rate was ∼0.4 cts s^{-1}. Although the count rate was not large enough to produce pile-up, we verified by removing the bright core (2–4″ in radius) and found that there was no significant spectral change and thus no pile-up. We also analyzed archival *Chandra* and *XMM-Newton* observations in order to see if there is a long term spectral variability in the soft band and to combine them with the *NuSTAR* observation to have a better spectral sensitivity in the soft band.

We first fit the *Swift* data alone to see if there was any spectral change in the soft band (0.5–10 keV) since the last *Chandra* or *XMM-Newton* measurements made ∼12 years ago (e.g., Morii et al. 2003). We grouped the spectrum to have 20 counts per bin for the fit. We first fit the data with an absorbed blackbody plus power-law model to compare with the archival *XMM-Newton* and *Chandra* data. The spectrum was a little harder than but consistent with previous results (Morii et al. 2003) as well as with our reanalysis of *XMM-Newton*+*Chandra* data (see Table 2). Therefore, all four observations could be combined with the *NuSTAR* observation, and we report fit results for the combined data.

We then tied all the model parameters between *NuSTAR*, *Swift*, *XMM-Newton*, and *Chandra* except for the cross-normalization factors (set to 0.9 for *NuSTAR*; the PSF correction factor) to fit the broadband spectrum (0.5–79 keV). To fit the data, we grouped the spectra to have at least 100 and 20 counts per bin for *NuSTAR* and the soft-band instruments (*Swift*, *XMM-Newton*, and *Chandra*), respectively. We tried to fit the data simultaneously with a blackbody plus power-law model. In fitting, we used the 0.5–10 keV and the 3–79 keV data for the soft-band instruments and *NuSTAR*, respectively. The model was unacceptable, and adding one more component improved the fit significantly. Therefore, we fit the data to an absorbed blackbody plus broken power-law, `tbabs*(bbody + bknpow)`, or an absorbed blackbody plus two power laws, `tbabs*(bbody+pow+pow)` in `XSPEC 12.7.1`. The former is to be compared with results of Kuiper et al. (2006) and the latter with those of Morii et al. (2010). We note that the blackbody component was required in both models. We summarize the results in Table 2.

We studied the effects of nonuniformity in the SNR background because the fit results may change depending on the background region used. For *NuSTAR*, which operates in the 3–79 keV band with a relatively broad PSF, effects of the thermal SNR and its spatial variation are likely to be very small. For other soft-band observatories, we first estimated the background to source count rates to be ∼15%, 6% and 5% for the *Swift*, *XMM-Newton* and *Chandra* data. Although variations on small background levels would not affect the spectral fit results much, the background level in the *Swift* data was relatively high, which may be a concern. Therefore, we used various background regions in the SNR for the spectral fits of the *Swift* and *XMM-Newton* data. As expected from the count rate estimates, *Swift* results fluctuate slightly (∼20–40% of the statistical uncertainties) depending on the background region used, but *XMM-Newton* results were more stable (∼6–20% of the statistical uncertainties). We then used the various *Swift* and *XMM-Newton* backgrounds for the joint fit of the *NuSTAR*, *Swift*, *XMM-Newton* and *Chandra* data, and found that the spectral variations caused by different backgrounds were typically $\lesssim$ 10% of the statistical uncertainties.

We find that our best-fit parameters for the absorbed blackbody plus two power-law model do not agree with those of Morii et al. (2010). We checked if the spectral model of Morii et al. (2010) is consistent with the *NuSTAR*, *Swift*, *XMM-Newton*, and *Chandra* data. We found that Morii et al. (2010) best-fit parameters do not describe our data. The null hypothesis probability was 7×10^{-4} (χ^2/dof=2601/2375) with a clear trend in the residuals at high energies ($\gtrsim$ 15 keV). We then varied their best parameters for the absorbed blackbody plus two power-law model ($N_{\rm H}$=2.836–2.896$\times10^{22}$ cm^{-2}, kT=0.496–0.576 keV, $\Gamma_{\rm s}$=4.39–5.59, $\Gamma_{\rm h}$=1.42–1.82) within the uncertainties (direct sum of the statistical and systematic uncertainties to maximize the parameter space) using the `steppar` command of `XSPEC` to see if we could find a set of parameters that is consistent with the data. The minimum χ^2/dof was 2530/2375, implying the null hypothesis probability of ∼0.01, and some of the best-fit parameters hit the limit, making the probability lower. We then limited the fit to the 0.5–60 keV range similar to the *Suzaku* data and still found that the Morii et al. (2010) best-fit parameters are inconsistent with our data. We therefore conclude that the X-ray spectrum of 1E 1841−045 we measured cannot be explained with the spectral model reported by Morii et al. (2010)

3.3. *Phase-Resolved and Pulsed Spectral Analyses*

We conducted a phase-resolved spectral analysis for three phase intervals, 0.15–0.5, 0.5–0.8, and 0.8–1.15 to catch distinct features in the pulse profiles (see Fig. 1 for pulse profiles). The temporal resolutions *Swift* XRT and *XMM-Newton* MOS are comparable to the phase intervals we use here, and spectral mixing between different

[4] http://www.swift.ac.uk/analysis/xrt/pileup.php

Table 2
Phenomenological spectral fit results for 1E 1841−045

Phase	Data[a]	Energy (keV)	Model[b]	$N_{\rm H}$ (10^{22} cm^{-2})	kT (keV)	$\Gamma_{\rm s}$[c]	$E_{\rm break}/F_{\rm s}$[d] (keV)	$\Gamma_{\rm h}$[e]	$F_{\rm h}$[f]	$L_{\rm BB}$[g]	χ^2/dof
0.0–1.0	S	0.5–10	BB+PL	2.23(25)	0.46(5)	1.76(39)	1.73(19)	···	···	1.58(29)	177/182
0.0–1.0	X,C	0.5–10	BB+PL	2.26(5)	0.42(1)	2.07(7)	1.74(5)	···	···	1.61(8)	1866/1849
0.0–1.0	N,S,X,C	0.5–79	BB+BP	2.24(4)	0.44(1)	2.09(4)	10.7(4)	1.33(3)	6.84(6)	1.91(8)	2440/2371
0.0–1.0	N,S,X,C	0.5–79	BB+2PL	2.58(10)	0.42(1)	2.96(18)	1.55(2)	1.06(9)	5.70(9)	1.24(21)	2427/2371
0.15–0.5	N,X,C	0.5–79	BB+BP	2.24[h]	0.44(1)	1.98(4)	12.4(9)	1.35(6)	7.50(7)	2.34(11)	819/797
0.5–0.8	N,X,C	0.5–79	BB+BP	2.24	0.44(1)	1.99(5)	12.6(8)	1.18(7)	7.78(9)	1.95(11)	687/652
0.8–0.15	N,X,C	0.5–79	BB+BP	2.24	0.45(1)	2.15(6)	10.0(5)	1.27(5)	5.79(7)	1.69(13)	606/633
0.15–0.5	N,X,C	0.5–79	BB+2PL	2.58	0.42(2)	2.99(13)	1.68(4)	1.19(10)	5.87(14)	1.51(26)	816/797
0.5–0.8	N,X,C	0.5–79	BB+2PL	2.58	0.45(4)	3.04(11)	1.51(4)	1.05(9)	6.45(16)	0.86(23)	680/652
0.8–0.15	N,X,C	0.5–79	BB+2PL	2.58	0.44(2)	2.91(11)	1.37(4)	0.91(11)	4.89(14)	1.33(22)	607/633
Pulsed[i]	X,C	0.5–10	PL	2.24	···	···	···	2.40(15)	0.43(4)	···	172/299
Pulsed	N,X,C	0.5–79	PL	2.24	···	···	···	1.98(7)	1.31(6)	···	429/640
Pulsed	N	5–79	PL	2.24	···	···	···	1.70(12)	1.58(15)	···	163/238
Pulsed	N	10–79	PL	2.24	···	···	···	1.36(23)	1.72(22)	···	79/114
Pulsed	N	15–79	PL	2.24	···	···	···	0.99(36)	1.76(27)	···	45/64

Notes. Uncertainties are at the 1σ confidence level. When combining data from different observatories, cross-normalization factors were used. The cross-normalization factors was set to 0.9 for module A of *NuSTAR* (see text), or 1 for *XMM-Newton* if *NuSTAR* data were not included. Fluxes were measured using the `cflux` model in `XSPEC`.
[a] N: *NuSTAR*, S: *Swift*, X: *XMM-Newton*, C: *Chandra*.
[b] BB: Blackbody, PL: Power law, BP: Broken power law.
[c] Photon index for the soft power-law component.
[d] Break energy for the broken power-law (BB+BP) fit or soft power-law flux (BB+2PL) in the 3–79 keV band if *NuSTAR* data were included. Otherwise, power-law flux in the 2–10 keV band in units of 10^{-11} erg cm^{-2} s^{-1}.
[e] Photon index for the hard power-law component.
[f] Absorption-corrected flux in units of 10^{-11} erg cm^{-2} s^{-1}. The values are only the power-law (hard power-law) flux in the 3–79 keV band for the BP (PL, 2PL) model when the *NuSTAR* data are included, otherwise power-law flux in the 2–10 keV band.
[g] Blackbody luminosity in units of 10^{35} erg s^{-1} for an assumed distance of 8.5 kpc.
[h] $N_{\rm H}$ for the phase-resolved and pulsed spectral analysis was frozen.
[i] `lstat` in `XSPEC` was used for fitting pulsed spectra, and we report L-Statistic/dof instead of χ^2/dof.

phases will occur, blurring the spectral differences among the phase intervals. Therefore, we ignored the *Swift* and *XMM-Newton* MOS data for the phase-resolved and pulsed spectral analysis below.

We binned the *NuSTAR* and the soft-band instruments' spectra to have 50 and 20 counts per spectral bin, respectively, and froze the cross normalizations to those obtained with the phase-averaged spectral fit. We fit the spectra with two models: an absorbed blackbody plus broken power-law and an absorbed blackbody plus double power-law model. We find that the spectra vary with spin phase, and the detailed variation depends on the spectral model used. We report the results in Table 2.

We also fit the pulsed spectrum after subtracting the unpulsed spectrum extracted in the phase interval 0.9–1.1. The *Chandra* and the *XMM-Newton* PN data were phase-aligned with the *NuSTAR* data by correlating the light curves. Since the number of pulsed source counts per spectral bin was small, we used `lstat` because the usual χ^2 method may bias the results. We then froze the cross normalizations between instruments to the values obtained with the phase-averaged spectral fits.

There were not many events in the pulsed spectra, and a simple power-law model could not be ruled out. However, we saw rising trends in the residuals in the soft band ($\lesssim$ 2 keV) and hard band ($\gtrsim$ 10 keV). Also motivated by the very hard power-law component ($\Gamma\sim0.7$) in the pulsed spectrum in the high energy band ($\sim$15–200 keV) reported by Kuiper et al. (2006), we gradually removed the soft bands from the spectral fit to see if the spectrum would become very hard above $\sim$15 keV, and found that indeed this occurred. We also tried to fit the data using alternative statistical methods (e.g., usual χ^2 method or `cstat` in `XSPEC`), and found that the alternative methods gave similar results except for the fit in the 0.5–79 keV band, where χ^2 results were significantly different from the others. The results are summarized in Table 2.

We also measured spectral pulsed fractions in the hard band (defined as ratios of pulsed and total fluxes) in order to compare to those reported by Kuiper et al. (2006). We first fit the total ($\gtrsim$ 11 keV) and the pulsed spectra ($\gtrsim$ 15 keV) to single pow-law models. The total spectrum above 11 keV was consistent with that we obtained using the absorbed blackbody plus broken power-law model (see Table 2). We then calculated the flux ratio (spectral pulsed fraction), and found it to be $24 \pm 4\%$ ($41 \pm 18\%$) at 20 keV (80 keV). The uncertainties were estimated by simulating both pulsed and total spectra using the covariance matrices obtained during the spectral fitting. Using 10,000 simulations, we calculated the flux ratios and the standard deviation to obtain the uncertainties.

Finally, we investigated the spectral properties of the double-peaked pulse profile in the 24–35 keV band (see Fig. 1). With the double-peaked structure decidedly significant (see Section 3.1), we searched for evidence for this structure in the spectra. We detect a possible excess (deficit) counts at $\sim$30 keV in the spectrum of phase 0.525–0.725 (0.325–0.525) but not in the spectra of the other phases. However, the continuum model alone is statistically acceptable and existence of an emission- or absorption-like feature cannot be clearly demonstrated with the present data.

3.4. *Spectral fits with the $e^{\pm}$ outflow model*

Next, we tested a new model proposed by Beloborodov (2013) to explain the hard X-ray emission from magnetars. The model envisions an outflow of relativistic electron-positron created by the pair discharge near the neutron star. The outflow moves along the magnetic field lines and gradually decelerates as it (resonantly) scatters the thermal X-rays. Its Lorentz factor decreases proportionally to the local magnetic field B,

$$\gamma \approx 100 \frac{B}{B_Q}, \tag{1}$$

where $B_Q = m_e^2 c^3/\hbar e = 4.44 \times 10^{13}$ G. This deceleration law determines the emitted spectrum of resonantly scattered photons. The outflow fills the active "j-bundle" of closed magnetospheric field lines (Beloborodov 2009). It radiates most of its kinetic energy in hard X-rays before the $e^{\pm}$ pairs reach the top of the magnetic loop and annihilate there.

In a simple geometry, the j-bundle is axisymmetric and emerges from the polar cap around the magnetic dipole axis of the star. In this case, the model has the following parameters: (1) the angular size of the polar cap, $\theta_{\rm j}$, (2) the power of the $e^{\pm}$ outflow along the j-bundle, L, (3) the magnetic dipole moment of the star, μ, (4) the angle between the rotation axis and the magnetic axis, $\alpha_{\rm mag}$, (5) the angle between the rotation axis and the observer line of sight, $\beta_{\rm obs}$, and (6) the reference point of the rotational phase, ϕ_0.

To test the model against data, we designed the following two-step method (Hascoët, R. et al., in preparation). First, we explore the entire parameter space by fitting the phase-averaged total (pulsed+unpulsed) spectrum and the phase-resolved pulsed spectra. At this step, we only consider data above 10 keV, where the outflow dominates the observed radiation. For 1E 1841−045 we used three phase bins for the phase-resolved spectra (Section 3.3). We found that the model successfully fits the data, with the best-fit $\chi^2/{\rm dof} = 1.13$ (for 267 dof); the obtained parameters of the model are given in Table 3. For the best-fit model, the emitted power peaks at ∼7 MeV. We also found a marginally acceptable (3σ confidence) second minimum ($\chi^2/{\rm dof} = 1.22$ for 267 dof). Both acceptable regions are well localized in the parameter space, and we show both solutions in Table 3.

At the second step, we freeze the best-fit parameters of the outflow model and fit the spectrum in the 0.5–79 keV band, using the *NuSTAR*, *Swift*, *Chandra* and *XMM-Newton* data. This allows us to analyze possible models for the soft X-ray component. We found that the data exclude the single-blackbody model. On the other hand, the data are well fitted by a blackbody plus power-law or by a two-blackbody model. The results are summarized in Table 4. Note that the outflow model spectrum extends down to low energies, and thus the soft-band spectral parameters are different from those obtained using the phenomenological models (see Table 2).

4. DISCUSSION

We have reported on X-ray observations of the magnetar 1E 1841−045, most notably on its high-energy X-ray properties as observed by *NuSTAR*. We find that the pulse profile in the ∼24–35 keV band shows a double-peaked structure, which was not reported previously. We also find that the rms pulsed fraction of the source is ∼20% at ∼50 keV. We show that the phase-averaged total spectrum of 1E 1841−045 can be modeled with an absorbed blackbody plus broken power-law or an absorbed blackbody plus two power-law model. Finally, we constrain the geometry of the source by fitting the phase-averaged and the phase-resolved spectra with the electron-positron outflow model of Beloborodov (2013).

Table 3
Best-fit parameters of the outflow model

Solution	$\alpha_{\rm mag}$ (rad)	$\beta_{\rm obs}$ (rad)	θ_j (rad)	$L^{\rm a}$	$\mu^{\rm b}$
1	0.3(2)	0.9(2)	< 0.4	5(1)	> 1.4
2	0.7(2)	1.4(1)	< 0.4	5(1)	> 1.4

[a]Outflow power in units of $10^{36}(D/8.5\ {\rm kpc})^2$ erg s^{-1}.
[b]Magnetic dipole moment in units of 10^{32} G cm^3.

4.1. *Pulse Profile*

The pulse profiles measured with *NuSTAR* broadly agree with those previously measured with *RXTE* (Kuiper et al. 2004). However, we note some differences. In the 7.8–11.7 keV band, the previously measured profile had a flat top, from which Kuiper et al. (2004) suggested that the dominance of the two pulses (one at phase ∼0.3 and the other at ∼0.7) changes at ∼9 keV. In the *NuSTAR* observation, the flattening occurred at 11.7–16.1 keV, implying the change occurred at ∼11 keV, similar to the location of the spectral break (see Table 2). Temporally measuring the exact energy over which the flattening occurs was difficult, and the difference between ∼9 keV and ∼11 keV may be marginal.

We found a double-peaked structure in the ∼24–35 keV band. It is not unusual for a magnetar's pulse profiles to change with energy. For example, den Hartog et al. (2008a) and den Hartog et al. (2008b) showed that the pulse profiles of two magnetars, AXP 1RXS J170849−400910 and AXP 4U 0142+61, change with energy. Furthermore, the two magnetars have separate peaks in their pulse profiles that correspond to the soft- and hard-band emission, respectively. It seems that the soft-emission peak leads the hard one in phase at least for those two magnetars (when considering the pulse minimum as phase 0). Although we could not clearly identify a hard peak at higher energies for 1E 1841−045, the peak at phase ∼0.6 in the 24–35 keV band may be its counterpart; our phase-resolved spectral analysis suggests this (see Table 2). If this is correct, 1E 1841−045 behaves similarly to AXP 1RXS J170849−400910 and AXP 4U 0142+61; the soft-emission peak leads the hard one (see also Göğüş et al. 2010, for SGR 0501+4516). It will be interesting to see if this trend is common to other magnetars.

The pulsed fraction of the source is known to increase with energy (Kuiper et al. 2006; Morii et al. 2010) and we confirm this (see Fig. 2). Furthermore, Kuiper et al. (2006) reported that the pulsed fraction of 1E 1841−045 is ∼25% at 20 keV, and ∼100% above ∼100 keV. Note that the rms pulsed fractions are shown in Figure 2, and they cannot be directly compared to those reported by Kuiper et al. (2006). Instead, we used the spectral pulsed fraction (Section 3.3) for the comparison. We found that the spectral pulsed fractions are $24 \pm 4\%$ at 20 keV, and $41 \pm 18\%$ at 80 keV. While they may be consistent with

Table 4
Spectral fit results for the soft component of 1E 1841−045 using the outflow model

Model[a]	$N_{\rm H}$ (10^{22} cm^{-2})	kT_1 (keV)	kT_2 (keV)	Γ[b]	F[c]	$L_{\rm BB,1}$[d]	$L_{\rm BB,2}$[d]	χ^2/dof
BB+PL	2.90(8)	0.55(2)	···	3.79(11)	0.55(4)	1.08(10)	···	2316/2272
BB+BB	2.03(4)	0.45(1)	0.90(4)	···	···	2.15(7)	0.65(9)	2298/2272
BB	1.72(2)	0.57(1)	···	···	···	2.15(4)	···	2556/2274

[a] BB: Blackbody, PL: Power law.
[b] Photon index for the power-law component.
[c] Absorption-corrected flux of the power law in units of 10^{-11} erg cm^{-2} s^{-1}, in the 3–79 keV band.
[d] Blackbody luminosity in units of 10^{35} erg s^{-1} for an assumed distance of 8.5 kpc.

those of Kuiper et al. (2006), they may agree better with a reanalysis of the *RXTE* and *INTEGRAL* data including more exposure (Kuiper, L., Hermsen, W. & Beek, F. in preparation).

4.2. *Spectrum*

We found that the spectral parameters of Morii et al. (2010) are inconsistent with those we obtained using the *NuSTAR*, *Swift*, *XMM-Newton*, and *Chandra* data. It is possible that the discrepancy between our results and those found using *Suzaku* is due to spectral variability in the source. However, the source is known to be fairly stable, at least in the soft band (Zhu et al. 2010; Lin et al. 2011; Dib & Kaspi 2013). Morii et al. (2010) noted that the point spread function of *Suzaku* is broad (HPD=2′), and it was difficult to subtract the Kes 73 background. Indeed, they used a supernova remnant (SNR) model obtained with *Chandra* for the Kes 73 background instead of directly subtracting the background. This may pose a problem in the soft band because the *Chandra* SNR model fit was not very good, as previously noted by Zhu et al. (2010); residuals in the Kes 73 model fit would be attributed to 1E 1841−045 spectrum. We independently checked if the Kes 73 model (`vsedov` used by Morii et al. 2010) fit the *Chandra* and *XMM-Newton* data well, and found that reduced χ^2 values for the model were ∼1.3–2.3, leaving significant residuals after the fit. Moreover, the number of SNR background events is estimated to be ∼70% larger than that of the source events for a circle of radius 110″ in the *XMM-Newton* data. Therefore, any residuals in the Kes 73 model fits will be amplified unless the source extraction region was small, which Morii et al. (2010) could not do because of the large HPD of *Suzaku*.

Morii et al. (2010) argued that the residuals are present only at the Kes 73 emission lines and will not affect the continuum model of the point source. It is not clear if the residuals are really only at the emission lines (for example, see their Fig. 2) and even if so, it is not clear that they do not affect the results for such a complicated point source spectral model.

Both BB+BP and BB+2PL models are phenomenological, and we use them mainly for comparison with previous data analyses. Although both provide a good fit to our data, BB+BP is more consistent with observations above 80 keV by Kuiper et al. (2006), who found $\Gamma_{\rm h} = 1.32$. Note that our analysis results support the anti-correlation between $\Gamma_{\rm s}-\Gamma_{\rm h}$ and B reported by Kaspi & Boydstun (2010), and a correlation between hardness ratio ($F_{\rm h}/F_{\rm s}$, ratio of hard to soft spectral component flux in the 1–60 keV band) and the characteristic age inferred from the spin-down rate by Enoto et al. (2010).

We note that the soft-band spectrum measured with *Swift* in 2012 November is consistent with those measured by *XMM-Newton* and *Chandra* 12 years ago. It has been suggested that the soft-band spectrum of the source has been stable over 13 years between 1993 and 2007 (Zhu et al. 2010). This is in spite of numerous spin-up glitches and bursts observed from this source (Dib et al. 2008; Lin et al. 2011). Our observations support this, in agreement with the results of Dib & Kaspi (2013) which are based only on the pulsed flux.

We found a hint of spectral excess (deficit) at ∼30 keV in the phase interval which corresponds to the pulse peak (dip) of the 24–35 keV pulse profile (see Fig. 1). If we interpret this as an electron (proton) cyclotron line, the inferred magnetic-field strength would be $\sim 3\times10^{12}$ G ($\sim 5\times10^{15}$ G). The magnetic-field strength for the electron cyclotron line is similar to those in the zone where the outflowing plasma radiates all its energy (Beloborodov 2013). Although the excess (deficit) might be produced by line emission (absorption), longer observations are required to demonstrate this.

With our 48-ks *NuSTAR* observation, the measurement of the pulsed spectrum in the hard X-ray band is not very precise. The obtained spectral slope in the 15–79 keV range is $\Gamma = 0.99 \pm 0.36$. It is consistent with $\Gamma = 0.72 \pm 0.15$ observed by *RXTE* and *INTEGRAL* in the 15–200 keV range (Kuiper et al. 2006). Morii et al. (2010) reported a different index of the pulsed spectrum, $\Gamma = 2.45^{+0.20}_{-0.21}$. Note, however, that they used a different energy band of 0.7–25 keV, heavily weighted in the soft band (< 10 keV), and thus more representative of the soft-band spectrum. When we limit our analysis to the 0.5–25 keV band with an $N_{\rm H}$ value of 2.87×10^{22} cm^{-2} (similar to those of Morii et al. 2010), we find $\Gamma = 2.19 \pm 0.09$, consistent with Morii et al. (2010). Although we argued above that the *Suzaku* spectral results might have been biased by Kes 73 contamination, the situation for the pulsed spectrum is different, because the Kes 73 spectrum is subtracted in a model-independent way when subtracting the DC component. Therefore the agreement with *Suzaku* results for the pulsed spectrum is unsurprising.

When limiting the analysis to the 2–25 keV band with an $N_{\rm H}$ value of 2.54×10^{22} cm^{-2} (similar to those used by Kuiper et al. 2006), the photon index became 2.00 ± 0.08, consistent with 1.98 ± 0.02, the value reported by Kuiper et al. (2006).

4.3. *Outflow model*

We found that the phase-resolved spectrum of 1E 1841−045 is consistent with the model of Beloborodov (2013). In this model, the X-ray emission comes from the active j-bundle filled with a relativistic $e^{\pm}$ outflow, whose Lorentz factor decreases according to Equation (1). The best-fit physical parameters are in agreement with the-

oretical expectations. Specifically, the active j-bundle is constrained to emerge from a polar cap of angular size $\theta_j \approx 0.4$, and the outflow power is measured to be $L \approx 5 \times 10^{36} (D/8.5\ \mathrm{kpc})^2\ \mathrm{erg\ s^{-1}}$. Using Equation (48) in Beloborodov (2009), one can estimate the voltage of $e^{\pm}$ discharge in the magnetosphere of 1E 1841−045. It gives $\Phi \approx 10^{10}\, \psi^{-1}$ V, where $\psi \sim 1$ radian is the magnetic twist implanted in the j-bundle, and we have used the magnetic moment of the neutron star $\mu \approx 7 \times 10^{32}$ G cm^3, which was estimated from the spin-down rate (Dib et al. 2008). The obtained voltage is in the expected range of $10^9 - 10^{10}$ V (Beloborodov & Thompson 2007).

The outflow power L must be equal to the bolometric luminosity emitted in hard X-rays. The best-fit model shows that the emitted power peaks at ∼7 MeV, outside the *NuSTAR* energy range. The exact location of the peak changes depending on the solution (Table 3), but is still in the MeV band. This is consistent with previous observations by *INTEGRAL* and *RXTE* (Kuiper et al. 2006). Our analysis also gives constraints on the geometry of the magnetized rotator in 1E 1841−045 (see Table 3), which may be tested and refined by future measurements of X-ray polarization (or radio polarization, if the source one day becomes radio bright), or by incorporating future modelling of the pulse profile.

We find that the hard X-ray emission from the $e^{\pm}$ outflow extends below 10 keV and must be included in the analysis of the soft X-ray component. When this contribution is taken into account, we find that (1) a single blackbody does not provide a good fit for the soft X-ray emission, (2) a two-temperature blackbody provides the best fit, and (3) a good fit is also provided by a blackbody plus power law model (Table 4).

The two-temperature blackbody model admits a simple physical interpretation. The cold blackbody $kT_1 \approx 0.45$ keV corresponds to the main thermal emission of the neutron star, and the hot blackbody $kT_2 \approx 0.9$ keV comes from a hot spot. The inferred emission areas of the cold and hot blackbodies are $\mathcal{A}_1 \sim \mathcal{A}_{\rm NS}/2$ and $\mathcal{A}_2 \sim 10^{-2}\mathcal{A}_{\rm NS}$, where $\mathcal{A}_{\rm NS}$ is the area of the neutron star surface (assuming radius $R_{\rm NS} = 10$ km). Interestingly, $\mathcal{A}_2$ is comparable to the area of the j-bundle footprint $\mathcal{A}_j \approx \pi \sin^2\theta_j R_{\rm NS}^2$. The footprint is expected to be hotter than the rest of the stellar surface, as it can be bombarded by the particles flowing in the j-bundle toward the neutron star. Similar hot spots were reported in transient magnetars (e.g., Gotthelf & Halpern 2007), but were not identified in bright persistent sources similar to 1E 1841−045.

The soft X-ray component could also be modeled as a single blackbody modified by resonant scattering in the magnetosphere (Thompson et al. 2002). Such a modification may be expected from scattering by the decelerated, mildly relativistic $e^{\pm}$ pairs in the equatorial region of magnetosphere (Beloborodov 2013). The effect is, however, currently difficult to model, because it is sensitive to the poorly understood velocity distribution of the highly opaque $e^{\pm}$ plasma near the magnetic equatorial plane.

5. CONCLUSIONS

We have analyzed 48-ks *NuSTAR* and simultaneous 18-ks *Swift* observations, and archival data from *XMM-Newton* and *Chandra* for the magnetar 1E 1841−045. To compare with previous observations we fit the source spectra with two phenomenological models: an absorbed blackbody plus broken power-law and an absorbed blackbody plus two power laws. The measured spectral parameters are consistent with those reported by Kuiper et al. (2006), and the photon index in the hard X-ray band is better constrained with the *NuSTAR* data than before. However, the *NuSTAR* data are not consistent with the spectral parameters reported by Morii et al. (2010). Although it is possible that the source might have varied since the *Suzaku* observations, it seems likely that an imperfect Kes 73 model caused problems in the background subtraction of the *Suzaku* data.

Our measurements of the pulsed spectrum are less constraining than but consistent with those in Kuiper et al. (2006). The pulsed spectrum is also consistent with *Suzaku* observations. We measured the rms pulsed fraction to be ∼20% at ∼50 keV. Although the pulsed fractions measured with spectra were not well constrained at high energies, it suggests that pulsed fraction may be lower than 100% at 100 keV.

We find that the pulse profile in the ∼24–35 keV band shows a double-peaked structure, which was not previously reported. The deviation of the pulse profile localized in a narrow energy range suggests a possible absorption (or emission) feature in the phase-resolved spectrum. Although we find some evidence for such a feature, it not statistically significant in the present data and requires deeper observations for possible confirmation.

The phase-resolved spectrum of 1E 1841−045 is consistent with the emission model of Beloborodov (2013). From the fit by the model we obtained constraints on the angle between the rotation and magnetic axes of the neutron star. We also inferred the size of the active j-bundle, the power of the $e^{\pm}$ flow, and the voltage of the $e^{\pm}$ discharge, all of which agree with theoretical expectations. The results imply that the object luminosity peaks at ∼7 MeV. Using this model, we place constraints on geometrical properties of the magnetar that in principle can be tested with future observations.

Using the physical model for the hard X-ray emission, we revisited the analysis of the soft X-ray component. We found that its phase-averaged spectrum can be fitted by two blackbodies, and the hot blackbody area is consistent with that expected for the footprint of the active j-bundle. However, we cannot rule out a power law plus blackbody for the soft component; future deeper observations may help in this regard.

This work was supported under NASA Contract No. NNG08FD60C, and made use of data from the *NuSTAR* mission, a project led by the California Institute of Technology, managed by the Jet Propulsion Laboratory, and funded by the National Aeronautics and Space Administration. We thank the *NuSTAR* Operations, Software and Calibration teams for support with the execution and analysis of these observations. This research has made use of the *NuSTAR* Data Analysis Software (NuSTARDAS) jointly developed by the ASI Science Data Center (ASDC, Italy) and the California Institute of Technology (USA). V.M.K. acknowledges support from an NSERC Discovery Grant, the FQRNT Centre de Recherche Astrophysique du Québec, an R. Howard Webster Foundation Fellowship from the

Canadian Institute for Advanced Research (CIFAR), the Canada Research Chairs Program and the Lorne Trottier Chair in Astrophysics and Cosmology. A.M.B. acknowledges the support by NASA grants NNX10AI72G and NNX13AI34G.

REFERENCES

Baring, M. G., & Harding, A. K. 2007, Ap&SS, 308, 109
Beloborodov, A. M. 2009, ApJ, 703, 1044
Beloborodov, A. M. 2013, ApJ, 762, 13
Beloborodov, A. M., & Thompson, C. 2007, ApJ, 657, 967
Capalbi, M., Perri, M., Saija, B., Tamburelli, F., & Angelini, L. 2005, The Swift XRT Data Reduction Guide, Technical Report 1.2
de Jager, O. C., Swanepoel, J. W. H., & Raubenheimer, B. C., et al. 1989, A&A, 221, 180
den Hartog, P. R., Kuiper, L., & Hermsen, W. 2008, A&A, 489, 263
den Hartog, P. R., Kuiper, L., Hermsen, W., & et al. 2008, A&A, 489, 245
Dib, R., & Kaspi, V. M. 2013, ApJ, submitted
Dib, R., Kaspi, V. M., & Gavriil, F. P. 2008, ApJ, 673, 1044
Duncan, R. C., & Thompson, C. 1992, ApJ, 392, L9
Enoto, T., Nakazawa, K., Makishima, K., & et al. 2010, ApJ, 722, L162
Gonzalez, M. E., Dib, R., Kaspi, V. M., Woods, P. M., Tam, C.R. & et al. 2010, ApJ, 716, 1345
Gotthelf, E. V. & Halpern, J. P. 2007, Ap&SS, 308, 79
Göğüş, E., Woods, P. M., Kouveliotou, C. & et al. 2010, ApJ, 722, 899
Hailey, C. J., An, H., Blaedel, K. L., et al. 2010, Proc. SPIE, 7732, 77320T
Harrison, F. A., Cook, W. R., Miyasaka, H., & McLean, R. Semiconductor Radiation Detection Systems, CRC press, 2010
Harrison, F. A., Craig, W. W., Christensen, F. E., et al. 2013, ApJ, 770, 103
Heyl, J. S., & Hernquist, L. 2005, ApJ, 618, 463
Kaspi, V. M., & Boydstun, K. 2010, ApJ, 710, L115
Kouveliotou, C., Dieters, S., Strohmayer, T. & et al. 1998, Nature, 393, 235
Kuiper, L., Hermsen, W., den Hartog, P. R., & Collmar, W. 2006, ApJ, 645, 556
Kuiper, L., Hermsen, W., & Mendez, M. 2004, ApJ, 613, 1173
Lin, L., Kouveliotou, C., Göğüş, E. et al. 2011, ApJ, 740, L16
Livingstone, M. A., Scholz, P., Kaspi, V. M., Ng, C.-Y., & Gavrill, F. P. 2011, ApJ, 743, L38
Mereghetti, S. 2008, A&A Rev., 15, 255
Molkov, S. V., Cherepashchuk, A. M., Lutovinov, A. A., et al. 2004, Sov. Astron. Lett., 30, 534
Morii, M., Kitamoto, S., Shibazaki, N., et al. 2010, PASJ, 62, 1249
Morii, M., Sato, R., Kataoka, J. & kawai, N. et al. 2003, PASJ, 55, L45
Ransom, S. M., Eikenberry, S. S. & Middleditch, J. 2002, ApJ, 124, 1788
Rea, N., Esposito, P., 2011, in High-Energy Emission from Pulsars and their Systems, ed. D. F. Torres & N. Rea (Berlin: Springer), 247
Rea, N., Esposito, P., Turolla, R., et al. 2010, Science, 330, 944
Rea, N., Israel, G. L., Esposito, P., et al. 2012, ApJ, 754, 27
Scholz P., Ng, C. Y., Livingstone, M., et al. 2012, ApJ, 761, 66
Thompson, C., & Beloborodov, A. M., 2005, ApJ, 634, 565
Thompson, C., & Duncan, R. C., 1996, ApJ, 473, 322
Thompson, C., Lyutikov, M., & Kulkarni, S. R. 2002, ApJ, 574, 332
Tian, W. W., & Leahy, D. A., 2008, ApJ, 677, 292
Vasisht, G., & Gotthelf, E. V. 1997, ApJ, 486, L129
Wachter, S., Patel, S. K., Kouveliotou, C., et al. 2004, ApJ, 615, 887
Wang, Q. D., & Gotthelf, E. V. 1998, ApJ, 494, 623
Woods, P. M., & Thompson, C. 2006, in Compact Stellar X-ray Sources, ed. W. H. G. Lewin & M. van der Klis (Cambridge University Press, UK, 2006)
Zhu, W., & Kaspi, V. M. 2010, ApJ, 719, 351

Prepared by LLNL under Contract DE-AC52-07NA27344